Research Square

Preprints are preliminary reports that have not undergone peer review.
They should not be considered conclusive, used to inform clinical practice,
or referenced by the media as validated information.

Green Synthesis of Silver Nanoparticles Using the Extract of Adenosma Caeruleum R.br.: Evaluation of Antibacterial, Antifungal and Antioxidant Activity

Van Son Nguyen

nguyenvanson@iuh.edu.vn

Industrial University of Ho Chi Minh City https://orcid.org/0000-0002-4951-0103

Thanh Cong Vo

Industrial University of Ho Chi Minh City

Thanh Khue Van

Industrial University of Ho Chi Minh City

The Ky Vo

Industrial University of Ho Chi Minh City

Research Article

Keywords: Silver nanoparticles, green synthesis, Adenosma caeruleum, antibacterial activity, antifungal activity, antioxidant activity

Posted Date: April 17th, 2026

DOI: https://doi.org/10.21203/rs.3.rs-9234917/v1

License: This work is licensed under a Creative Commons Attribution 4.0 International License.
Read Full License

Version of Record: A version of this preprint was published at Applied Biochemistry and Biotechnology on July 6th, 2026. See the published version at https://doi.org/10.1007/s12010-026-05817-4.

GREEN SYNTHESIS OF SILVER NANOPARTICLES USING THE EXTRACT OF *ADENOSMA CAERULEUM* R.BR.: EVALUATION OF ANTIBACTERIAL, ANTIFUNGAL AND ANTIOXIDANT ACTIVITY

Van Son Nguyen[*, 1], Thanh Cong Vo[1],Thanh Khue Van[1], The Ky Vo[1]
[1]Faculty of Chemical Engineering, Industrial University of Ho Chi Minh City, Ho Chi Minh City, Viet Nam
Corresponding author: nguyenvanson@iuh.edu.vn

Abstract. Silver nanoparticles (AgNPs) have garnered considerable interest owing to their outstanding antimicrobial and antioxidant performances. In the present work, AgNPs were greenly synthesized using *Adenosma caeruleum* R.Br. extract, which simultaneously acted as reducing and capping agents, providing an environmentally benign and sustainable route for nanoparticle production. The influence of key synthetic variables, including $AgNO_3$ concentration, extract-to-precursor ratio, temperature, pH, and reaction time, was systematically optimized to achieve well-dispersed and stable nanostructures. Comprehensive physicochemical characterization by UV–Vis, FT-IR, XRD, DLS, zeta potential, TEM, and EDS confirmed the successful formation of crystalline, predominantly spherical AgNPs with core sizes in the range of 20–50 nm and an average hydrodynamic diameter of ~47.5 nm, indicative of good colloidal stability imparted by phytochemical capping layers. The biosynthesized AgNPs exhibited notable radical-scavenging activity toward $ABTS^{\bullet+}$ with an IC_{50} value of 49.8 μg mL^{-1}, demonstrating a moderate yet meaningful antioxidant capacity. Significant antimicrobial efficacy was also observed in the agar well diffusion assay (30 μL), producing inhibition zones of 21.0 mm (*Escherichia coli*), 14.0 mm (*Bacillus cereus*), 22.0 mm (*Salmonella typhimurium*), 14.0 mm (*Staphylococcus aureus*), and 12.0 mm (*Candida albicans*), where Gram-negative bacteria were generally more susceptible. The minimum inhibitory concentration was 1.25 mg mL^{-1} for all tested strains. Overall, these findings demonstrate that *A. caeruleum*-mediated AgNPs possess promising antibacterial, antifungal, and antioxidant properties, highlighting their strong potential for future biomedical and environmental applications.

Keywords: Silver nanoparticles, green synthesis, *Adenosma caeruleum*, antibacterial activity, antifungal activity, antioxidant activity

1. INTRODUCTION

The rapid emergence of antimicrobial-resistant microorganisms has become a serious global challenge, threatening public health and environmental safety. The excessive and prolonged use of conventional antibiotics has significantly reduced their effectiveness, leading to increased treatment failure and mortality rates [1,2]. Consequently, the development of alternative antimicrobial agents that are effective, safe, and environmentally sustainable has become an urgent research priority [3].

Nanotechnology has opened new opportunities in addressing these challenges by enabling the design of functional nanomaterials with enhanced physicochemical and biological properties [4]. Among various metal-based nanomaterials, silver nanoparticles (AgNPs) have attracted particular attention due to their broad-spectrum antibacterial, antifungal, and antiviral activities, even at low concentrations [5,6]. The antimicrobial efficacy of AgNPs is mainly attributed to their nanoscale size, high surface-to-volume ratio, and ability to release Ag^+ ions, which disrupt microbial cell membranes, interfere with intracellular proteins and DNA, and induce oxidative stress [7–9]. Owing to these properties, AgNPs have been widely explored for applications in wound dressings, medical devices, water treatment, food packaging, and biomedical coatings [10,11].

Conventional synthesis methods for AgNPs, including chemical reduction, photochemical, electrochemical, and microemulsion techniques, have been extensively reported [12]. However, these approaches often require toxic reducing agents such as sodium borohydride or hydrazine, high energy input, and strict reaction conditions, raising concerns regarding environmental impact, cost, and biocompatibility [13,14]. In response to these limitations, green synthesis strategies based on the principles of sustainable chemistry have gained increasing interest [15].

Green synthesis of AgNPs using biological resources represents an eco-friendly and cost-effective alternative to traditional methods. Among biological approaches, plant-mediated synthesis has emerged as a particularly attractive route due to its simplicity, rapid reaction kinetics, scalability, and elimination of the need for sterile conditions [16,17]. Plant extracts are rich in bioactive phytochemicals, such as flavonoids, phenolic acids, terpenoids, alkaloids, and coumarins, which can simultaneously act as reducing and stabilizing agents during nanoparticle formation [18]. Moreover, AgNPs synthesized using plant extracts often exhibit enhanced biological activities owing to synergistic effects between metallic silver and surface-bound phytochemicals [19].

Adenosma caeruleum R.Br. (as shown in Figure 1), commonly known as Nhân trần, is a medicinal plant widely distributed in Vietnam and other Southeast Asian countries. It has long been used in traditional medicine for liver protection, detoxification, anti-inflammatory, and antimicrobial

purposes [20]. Phytochemical studies have revealed that *A. caeruleum* contains various biologically active compounds, including quercetin, scopoletin, and other phenolic constituents, which possess antioxidant and antimicrobial properties [21–23]. These compounds suggest a strong potential for *A. caeruleum* extract to function as an effective bioreducing and stabilizing agent in the green synthesis of metal nanoparticles.

Despite the well-documented medicinal value of *A. caeruleum*, its application in the biosynthesis of silver nanoparticles remains limited. In particular, systematic investigations focusing on the optimization of synthesis parameters, physicochemical characterization, and comprehensive evaluation of antibacterial, antifungal, and antioxidant activities of *A. caeruleum*-mediated AgNPs are still scarce. Furthermore, studies that correlate green synthesis conditions with multifunctional biological performance are rarely reported.

Therefore, the present study aims to develop an eco-friendly green synthesis of silver nanoparticles using *Adenosma caeruleum* leaf extract as both reducing and stabilizing agents. The effects of key synthesis parameters, including $AgNO_3$ concentration, extract-to-metal salt ratio, pH, temperature, and reaction time, were systematically investigated to optimize nanoparticle formation. The synthesized AgNPs were characterized using UV–Vis spectroscopy, FT-IR, XRD, DLS, zeta potential, and EDS analyses. In addition, their antibacterial, antifungal, and antioxidant activities were evaluated to assess their potential for biomedical and environmental applications. This work contributes to the sustainable development of functional nanomaterials derived from indigenous medicinal plants and supports the growing interest in green nanotechnology.



Figure 1: *Adenosma caeruleum* R. Br.

2.1. MATERIALS AND METHODS

2.1.2. CHEMICALS

In this study, dried leaves of *A. caeruleum* harvested in October from the Central Pharmacy of Hoa Binh Province, Vietnam, were used as the natural source for the green synthesis of silver nanoparticles (AgNPs). The plant material was extracted under reflux with 70% ethanol. The resulting extract was filtered and concentrated to obtain a bioactive-rich solution, which was subsequently stored at 4 °C for further use. Only flowers with a bright yellow color and intact, pest-free petals were selected to ensure high-quality raw materials for the synthesis process. The silver ion (Ag^+) precursor solution was prepared from analytical-grade silver nitrate ($AgNO_3$, Sigma-Aldrich). All other reagents employed in the experiments were of analytical grade, ensuring the reliability and reproducibility of the synthesis.

2.1.2 Machine Equipment

UV–Vis spectra were recorded on a Thermo Gensys 10 spectrophotometer (190–1100 nm) to monitor the formation of AgNPs in aqueous dispersion. Functional groups of the dragon fruit peel extract involved in reduction and stabilization were analyzed by FT-IR spectroscopy (FT-IR-4700).

LC–MS measurements were performed using electrospray ionization with a capillary voltage of 3–5 kV. Nebulization with heated gas facilitated solvent evaporation and ion formation. Analyses were typically conducted at flow rates of 1–2 mL min^{-1}, while microbore columns (1–3 mm i.d., 50–200 μL min^{-1}) were used to enhance sensitivity.

X-ray diffraction patterns were obtained on a Bruker D8 Advance diffractometer with Cu Kα radiation over a 2θ range of 10–80°. Particle size distribution and zeta potential were determined using a Horiba SZ-100 analyzer. The isolated exosomes were characterized using transmission electronmicroscopy (TEM, H7650, Hitachi).

2.2. Prepare the extract

Adenosma caeruleum R. Br. was dried at 70 °C to constant weight and subsequently cut into small fragments. An amount of 10.0 g of the dried material was extracted with 200 mL of 70% ethanol. The mixture was heated to boiling and maintained under gentle reflux for 1 h to facilitate the extraction of phytochemicals. After cooling, the suspension was filtered to remove insoluble residues. A portion of the concentrated filtrate was subjected to LC–MS analysis to elucidate its

chemical constituents, while the remaining extract was employed for the biosynthesis of silver nanoparticles.

2.3. Green Synthesis of Silver Nanoparticles

AgNPs were synthesized by mixing the leaf extract with aqueous $AgNO_3$ solution under controlled conditions. The influence of $AgNO_3$ concentration (0.001–0.005 M), extract-to-$AgNO_3$ volume ratio, pH (6–9), temperature (30–80 °C), and reaction time was systematically investigated. The formation of AgNPs was initially confirmed by a visible color change and UV–Vis spectroscopy.

2.4. Investigation of free radical scavenging by ABTS

The antioxidant capacity of AgNPs was assessed using the $ABTS^{\cdot+}$ free radical scavenging assay. To prepare the $ABTS^{\cdot+}$ working solution, 20 μL of ABTS (7 μM) was mixed with 2.45 μM $K_2S_2O_8$ and allowed to react in the dark for 12–24 hours. The resulting solution was then diluted with ethanol to achieve an absorbance of 0.7 ± 0.02 at 734 nm. For the antioxidant activity evaluation, 25 μL of AgNP solution at varying concentrations (50, 100, 200, 300, and 400 μM) was added to 3 mL of the prepared $ABTS^{\cdot+}$ solution. After one minute of incubation, absorbance was measured at 734 nm. Trolox, at the same concentration range, was used as a positive control for calibration. After measuring the optical density values, a standard curve is constructed in the form:

$$Y = aX + b \quad (1)$$

The IC_{50} value was subsequently determined using the following formula:

$$IC_{50} = \frac{50-b}{a} \quad (2)$$

This equation calculates the concentration needed to achieve 50% inhibition using the standard curve, with parameters *a* and *b* determined in (1).

2.5. Antibacterial and Antifungal Assays

The antimicrobial performance of the AgNPs was evaluated against *Escherichia coli*, *Salmonella typhimurium*, *Staphylococcus aureus*, *Bacillus cereus*, and *Candida albicans* using agar diffusion and minimum inhibitory concentration (MIC) assays.

For the agar diffusion assay, the microbial inoculum was adjusted to a density of 10^6 CFU mL^{-1} and evenly spread over the agar surface using a sterile cotton swab. Wells were subsequently punched into the agar, and the test solutions were carefully loaded into each well. The plates were incubated at 34.9 °C for 24 h under appropriate conditions. A solvent blank was included on every

plate as the negative control. The sample layout was defined as follows: B1, positive control chloramphenicol); B2, negative control (H_2O); and A1–A3, test samples at concentrations of 30, 20, and 10 mg /mL, respectively (Fig. 2).

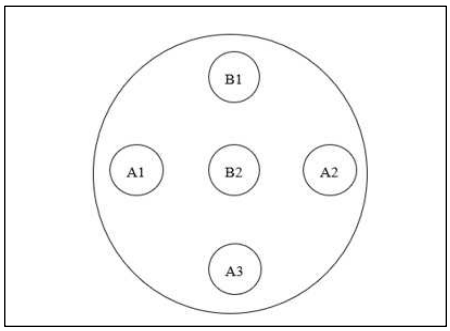


Figure 2. Antibacterial layout diagram

3. Results and discussion

3.1. LC-MS analysis results of the *Adenosma caeruleum* R. B extract

The LC–MS chromatogram of *Adenosma caeruleum* extract (**Fig**. 3 and **Table 1**) exhibited well-resolved peaks within the retention time range of 9.55–18.85 min, indicating a chemically diverse phytochemical profile. Peaks at RT 9.55–10.25 min (peaks 1–2) were tentatively assigned to phenolic acids, such as chlorogenic acid and caffeic acid, based on their retention behavior and the observed protonated molecular ions at m/z 355 and 181 ($[M+H]^+$), respectively.

A series of peaks at RT 10.66–11.90 min (peaks 3–5) were attributed to coumarins, including scopoletin (m/z 193 $[M+H]^+$), scoparone (m/z 223 $[M+H]^+$), and umbelliferone (m/z 163 $[M+H]^+$). Among these, the signal at RT 11.46 min was tentatively assigned to scoparone, a characteristic marker compound.

The most intense peak at RT 12.64 min (peak 6) was tentatively identified as a flavonoid glycoside, such as rutin (m/z 611 $[M+H]^+$), suggesting that glycosylated flavonoids are among the major constituents of the extract.

At longer retention times (RT 15.99–18.85 min; peaks 7–9), less polar flavonoid aglycones were detected, including quercetin (m/z 303 $[M+H]^+$), apigenin (m/z 271 $[M+H]^+$), and luteolin (m/z 287 $[M+H]^+$). These polyphenolic compounds, rich in hydroxyl and carbonyl

groups, are likely responsible for the reduction of Ag^{+} to Ag^{0} and subsequent stabilization of AgNPs.

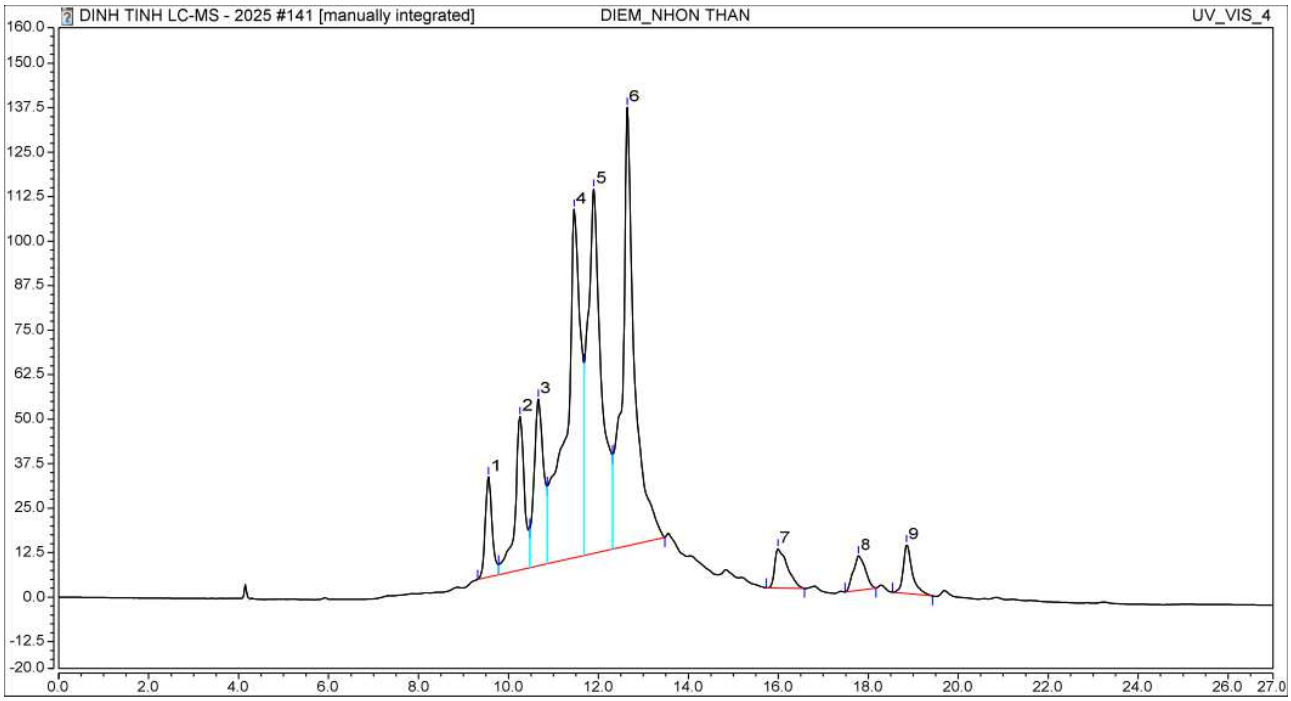
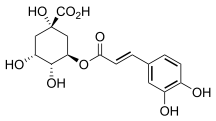
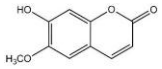
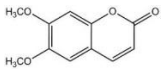
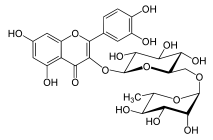
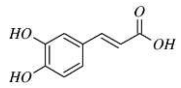
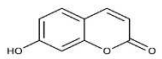
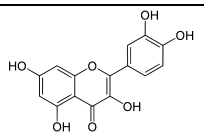
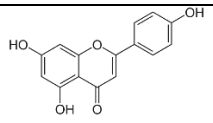
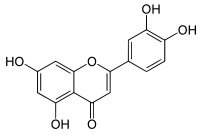


Figure 3. LC–UV chromatogram of the Artemisia capillaris extract monitored at 254 nm.

Table 1: Tentative assignment of major constituents in the *Artemisia capillaris* extract from LC–MS data

No.	Compd.	IUPAC name	Mol. formula	Structure	Mol. wt.
1	Chlorogenic acid	(1S,3R,4R,5R)-3-{[(2E)-3-(3,4-dihydroxyphenyl)prop-2-enoyl]oxy}-1,4,5-trihydroxycyclohexane-1-carboxylic acid	$C_{16}H_{18}O_9$		354.31
2	Scopoletin	7-hydroxy-6-methoxy-2H-1-benzopyran-2-one	$C_{10}H_8O_4$		192.17
3	Scoparone	6,7-dimethoxy-2H-1-benzopyran-2-one	$C_{11}H_{10}O_5$		222.19
4	Rutin	5,7-dihydroxy-2-(3,4-dihydroxyphenyl)-3-$(\alpha - L - rhamnopyranosyl) - (1 \rightarrow 6) - \beta - D - glucopyranosyloxy$-4H-chromen-4-one	$C_{27}H_{30}O_{16}$		610.52
5	Caffeic acid	(2E)-3-(3,4-dihydroxyphenyl)prop-2-enoic acid	$C_9H_8O_4$		180.16
6	Umbelliferone	7-hydroxy-2H-1-benzopyran-2-one	$C_9H_6O_3$		162.14
7	Quercetin	2-(3,4-dihydroxyphenyl)-3,5,7-trihydroxy-4H-chromen-4-one	$C_{15}H_{10}O_7$		**302.24**
8	Apigenin	5,7-dihydroxy-2-(4-hydroxyphenyl)-4H-chromen-4-one	$C_{15}H_{10}O_5$		270.24
9	Luteolin	2-(3,4-dihydroxyphenyl)-5,7-dihydroxy-4H-chromen-4-one	$C_{15}H_{10}O_6$		286.24

Importantly, the abundance of polyphenolic structures bearing hydroxyl and carbonyl functionalities provides a plausible chemical basis for the green synthesis of

AgNPs. These groups can participate in electron transfer processes, enabling the reduction of Ag^{+} ions to metallic Ag^{0}, while simultaneously adsorbing onto the nanoparticle surface to act as capping and stabilizing agents. In particular, flavonoids and phenolic acids, due to their redox-active nature, are expected to play a dominant role in both nucleation and growth stages, whereas coumarins may further contribute to surface functionalization and biological activity.

The concurrent occurrence of phenolic acids, coumarins, and flavonoids therefore implies potential synergistic interactions, which not only define the phytochemical profile of the extract but also rationalize its effectiveness in nanoparticle formation and the resulting bioactivity.

3.2. Survey results of factors affecting the synthesis process of nano Silver

3.2.1. Mechanism of Ag nanofabrication by *Adenosma caeruleum* extract

The extract of *Adenosma caeruleum* is enriched with flavonoids, phenolic acids, and related aromatic metabolites containing abundant hydroxyl and carbonyl functionalities (Table 1). These molecules are considered the key driving force for the conversion of Ag^{+} into metallic Ag^{0} via electron donation from phenolic groups, which are simultaneously oxidized to quinone-type structures.

The nanofabrication process can be interpreted through three consecutive stages: nucleation, growth, and stabilization. Initially, rapid reduction of Ag^{+} generates Ag^{0} atoms that collide to form small clusters, acting as primary nuclei. Once nuclei are formed, further reduced silver atoms deposit onto their surfaces, leading to particle growth. The rate of reduction, which is highly dependent on pH, governs the balance between nucleation and growth. Under mildly alkaline conditions, deprotonation of –OH groups increases the electron density of the ligands, accelerates Ag^{+} reduction, and promotes the formation of a large number of nuclei, ultimately yielding smaller and more uniformly distributed nanoparticles. This explains why the optimal synthesis efficiency was observed at pH 8.

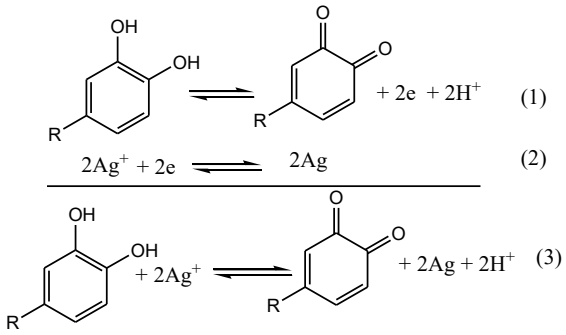


Fig. 4. Proposed redox mechanism of Ag^+ reduction and capping of AgNPs by *Adenosma caeruleum* phytochemicals.

Strong experimental evidence supporting this mechanism is provided by FTIR and LC–MS analyses. The FTIR spectra of the extract before and after reaction reveal noticeable changes in the intensity and position of characteristic bands associated with O–H stretching, C=O vibrations, and aromatic C=C groups, indicating their participation in the redox process and subsequent adsorption onto the nanoparticle surface. Meanwhile, LC–MS profiling confirms the presence of flavonoid and phenolic constituents capable of acting as both electron donors and surface ligands. The decrease or modification of signals corresponding to these compounds after nanoparticle formation further supports their involvement in reduction and capping.

Therefore, the biomolecules in *Adenosma caeruleum* extract not only initiate nucleation and regulate particle growth but also create an organic corona around the AgNPs, enhancing colloidal stability and preventing aggregation, as illustrated in Fig. 4.

3.2.2. Formation and optical behavior of AgNPs

The biosynthesis of AgNPs mediated by Artemisia capillaris extract was readily recognized from the rapid color transformation of the reaction medium from pale yellow to dark brown, indicating the reduction of Ag^+ to Ag^0 and the onset of surface plasmon resonance (SPR). The UV–Vis spectra consistently exhibited a characteristic absorption band in the visible region, whose intensity and profile sensitively reflected nanoparticle nucleation, growth, and colloidal stabilization.

Systematic variation of synthetic parameters revealed that precursor availability plays a decisive role in defining plasmonic behavior. As presented in Fig. 5a, the solution containing 0.0005 M $AgNO_3$ generated the most intense and relatively narrow SPR band, implying efficient formation of small and stabilized nanoparticles. Increasing the metal concentration resulted in gradual band broadening and a non-linear absorbance response, suggesting enhanced polydispersity and partial

aggregation due to insufficient surface protection. DLS analysis supports this interpretation by showing a wide size distribution mainly within 40–100 nm.

A similar kinetic tendency was observed when modulating the extract-to-precursor ratio (Fig. 5b). At low extract content, the limited supply of reducing equivalents slowed nucleation and produced weak plasmonic signals. Upon increasing the proportion of phytochemicals, the reduction rate accelerated and a burst formation of nuclei occurred, leading to stronger and sharper SPR features. At the ratio of 5:1, the spectrum became symmetric and stable, evidencing that metal atom generation and organic passivation were optimally synchronized.

Time-dependent measurements further clarified the evolution of the nanosystem (Fig. 5c). The rapid amplification of the SPR intensity during the early stage demonstrates fast establishment of a plasmonically active colloid. The maximum absorbance was reached at 60 min, at which nucleation and capping remained in balance. Prolonged reaction induced a slight attenuation and broadening of the band, attributable to coalescence and Ostwald ripening, in agreement with the enlarged hydrodynamic sizes observed by DLS and the reduced interparticle distance in TEM images.

Temperature exerted a comparable kinetic influence (Fig. 5d). Mild heating at 60 °C markedly enhanced the reduction efficiency and yielded a well-defined plasmon peak. Beyond this value, however, no improvement in intensity was obtained; instead, excessively rapid formation likely exceeded the stabilizing capacity of the biomolecular corona, promoting interparticle coupling and damping the optical response.

The pH of the medium governed the ionization state of phenolic and flavonoid groups, thereby modulating both electron transfer and adsorption onto the metallic surface. The most favorable plasmonic characteristics were achieved at pH 8 (Fig. 5e), where deprotonation enhances reducing power and ligand–metal coordination. More acidic conditions suppressed nucleation, whereas overly forcing environments tended to compromise colloidal integrity.

Taken together, all experimental variables converge toward a unified mechanistic picture: AgNP production is maximized when Ag^0 generation and phytochemical stabilization proceed cooperatively. The combination of 0.0005 M $AgNO_3$, an extract/precursor ratio of 5:1, a reaction

time of 60 min, a temperature of 60 °C, and pH 8 therefore provides the most favorable balance between nanoparticle yield, size uniformity, and dispersion stability.

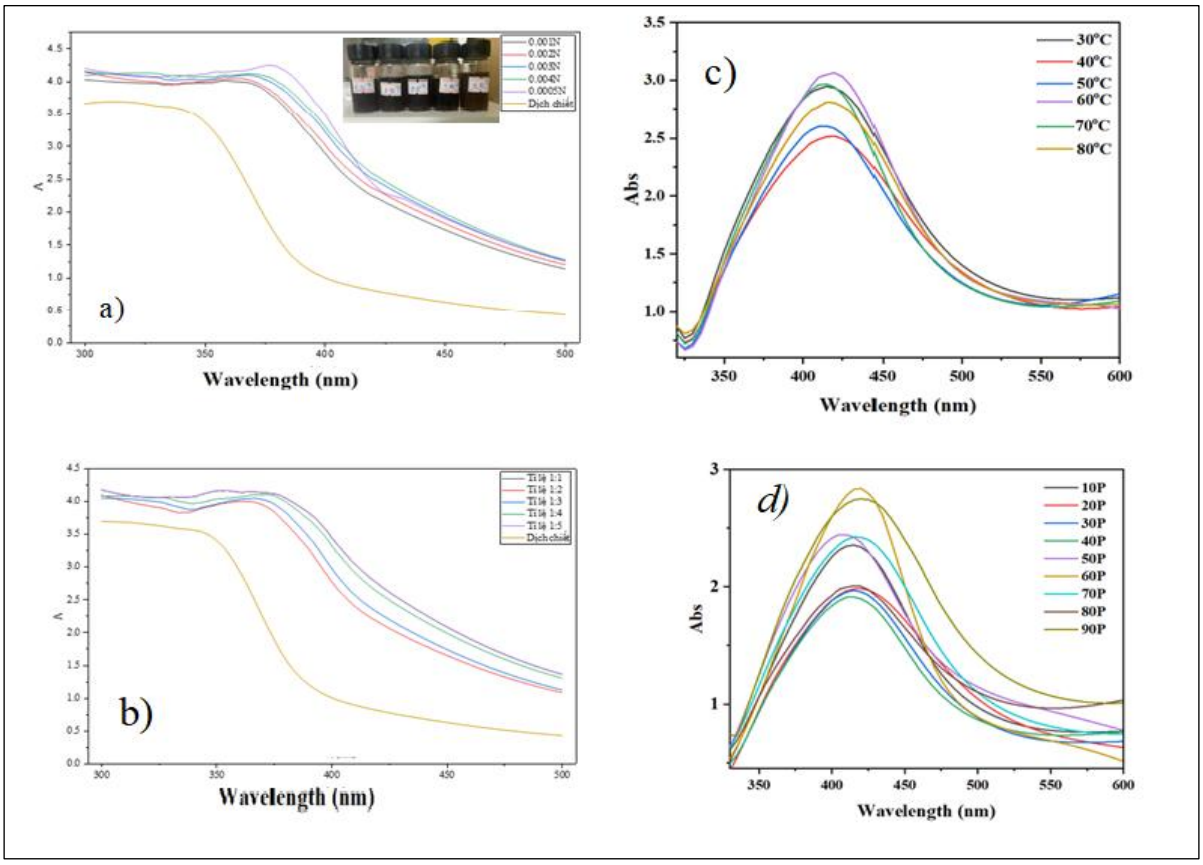


Fig. 5. UV–Vis spectra of AgNPs under different synthesis conditions: (a) surface plasmon resonance (SPR) at varying $AgNO_3$ concentrations; (b) evolution of SPR bands at different Artemisia capillaris extract/$AgNO_3$ ratios; (c) spectra of AgNP colloids obtained at different reaction temperatures; (d) temperature-mediated variation in SPR profiles.

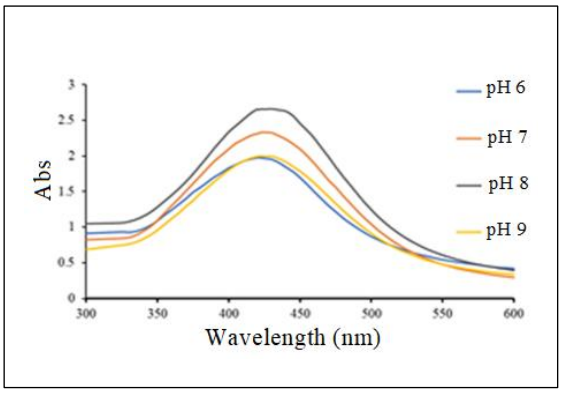


Fig. 5e. pH-dependent UV–Vis absorption spectra of the synthesized AgNPs

While UV–Vis spectroscopy provides rapid evidence for plasmon formation and offers indirect insight into nucleation kinetics and colloidal stability, it does not directly resolve particle morphology, crystalline organization, or surface chemistry. Therefore, a comprehensive structural investigation was undertaken to validate the optical interpretation. Electron microscopy was employed to visualize particle size and spatial distribution, X-ray diffraction (XRD) was used to determine phase purity and crystallinity, Fourier-transform infrared spectroscopy (FTIR) elucidated the involvement of phytochemical functional groups in reduction and capping, and energy-dispersive X-ray spectroscopy (EDX) confirmed the elemental composition of the nanosystem. Together, these complementary techniques enable correlation between plasmonic behavior and the physicochemical architecture of the biosynthesized AgNPs.

3.2.3. Structural characterization of the silver nanoparticles

The successful formation of silver nanoparticles mediated by *Adenosma caeruleum* extract was verified through a combination of optical, structural, morphological, and surface analyses. The appearance of the characteristic surface plasmon resonance band in the UV–Vis spectrum confirmed the rapid bioreduction of Ag^{+} ions into metallic Ag^{0}, indicating nucleation and growth of nanosized particles.

Direct visualization by TEM revealed predominantly discrete nanoparticles with dimensions in the nanometer regime, whereas DLS measurements (Figure 6c) provided insight into their hydrodynamic behavior in suspension. The distribution profile indicated a heterogeneous system in which most particles were concentrated within 20–100 nm, accompanied by a smaller fraction of aggregates extending to 100–250 nm. Such clustering can be attributed to interparticle association mediated by adsorbed phytochemicals, which may occasionally induce bridging effects. This interpretation is supported by the relatively high polydispersity index (PDI = 0.895), suggesting limited monodispersity and potential implications for long-term storage. Nevertheless, the Z-average diameter of 47.5 nm coincided with the dominant population, confirming that a substantial portion of the nanoparticles remained within a size range favorable for biological interactions.

To further evaluate colloidal stability, zeta potential analysis was performed (Figure 6d). The AgNPs exhibited a surface potential of -75.2 mV, a value typically associated with good electrostatic stabilization. The strong interparticle repulsion implied that the observed aggregates are more likely weak and reversible rather than irreversible coagulates. The origin of this surface

charge can be linked to ionizable functional groups from plant-derived molecules bound to the nanoparticle exterior.

The crystalline structure of the metallic core was unequivocally demonstrated by the XRD pattern (Figure 6b), which displayed intense reflections at $2\theta \approx 38.59°$, 44.87°, 64.37°, and 76.8°, corresponding respectively to the (111), (200), (220), and (311) planes of face-centered cubic silver. The sharp diffraction peaks confirmed the high crystallinity of Ag^0, in agreement with the plasmonic features detected by UV–Vis and the individual particles observed in TEM.

Beyond the inorganic framework, FTIR spectroscopy (Fig. 6a) elucidated the organic environment surrounding the nanoparticles. A broad band at 3419.63 cm^{-1} was assigned to O–H stretching vibrations of hydroxyl groups, characteristic of polyphenols and flavonoids known to donate electrons during Ag^+ reduction. The signal at 2925.88 cm^{-1} corresponded to C–H stretching, confirming the presence of organic chains on the surface. Meanwhile, the band at 1612.42 cm^{-1} (C=O/C=C) suggested partial oxidation of phenolic constituents and coordination between oxygen atoms and silver. Additional contributions from C–O/C–O–C vibrations at 1078.16 cm^{-1}, together with the Ag–O/Ag–OH feature at 646.12 cm^{-1}, provided direct evidence for metal–ligand interactions forming a stabilizing bio-organic corona.

The elemental composition obtained from EDS analysis (Fig. 7) reinforced this model. Silver accounted for 75.82 ± 5.67% of the material, confirming its dominance in the nanostructure, while carbon (15.71 ± 0.78%) and oxygen (8.47 ± 1.50%) originated from phytochemical residues adsorbed or coordinated at the surface. The characteristic Ag$L\alpha$, Ag$L\beta$, and AgM lines verified the presence of metallic silver, whereas the C K_α and O K_α peaks substantiated the existence of the organic shell previously identified by FTIR and inferred from the zeta potential.

Collectively, these complementary results converge toward a consistent structural picture: a highly crystalline Ag^0 core encapsulated within a layer of bioactive plant metabolites. This hybrid architecture ensures nanoscale dimensions, adequate dispersion stability, and a chemically active interface, thereby providing the physicochemical foundation for the antimicrobial and antioxidant performances discussed in the following section.

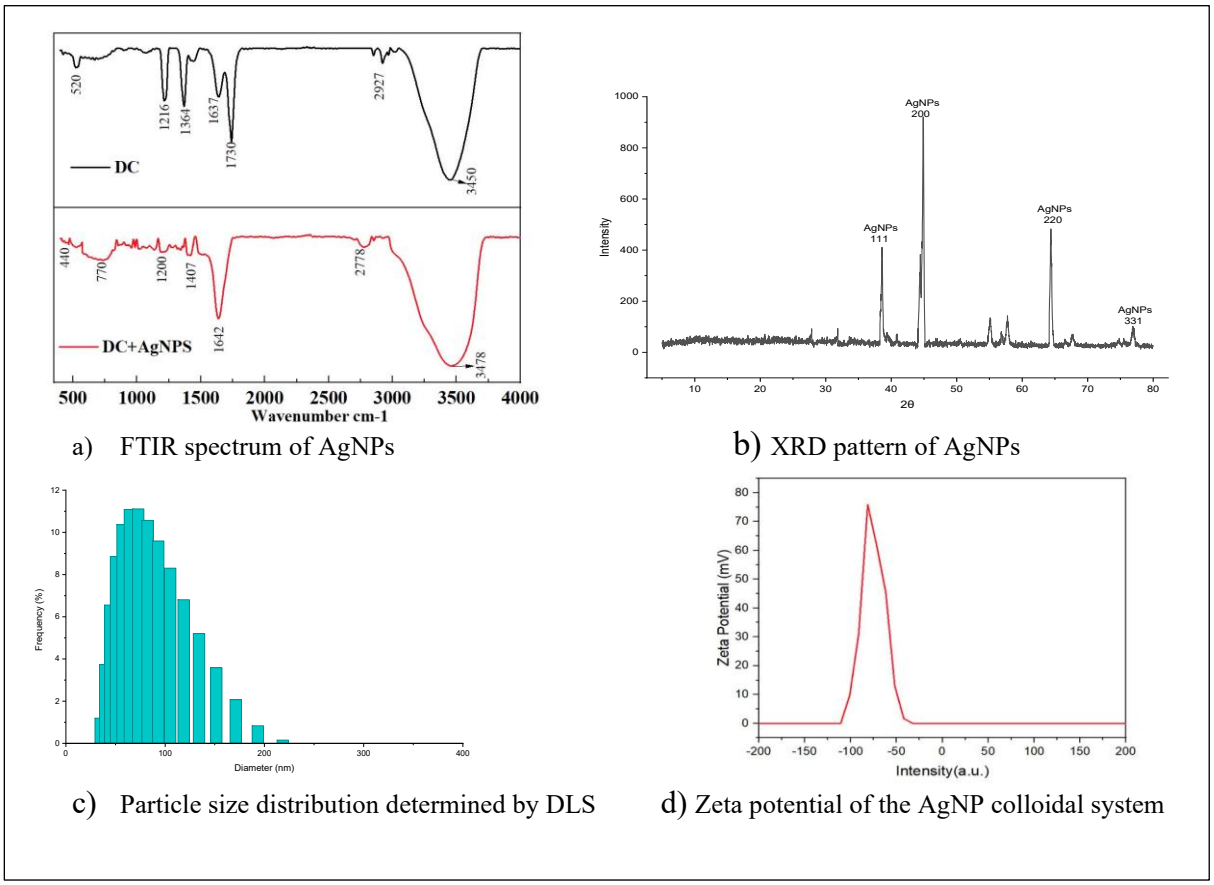


Fig. 6. (a) FTIR spectrum of AgNPs; (b) XRD pattern of AgNPs; (c) Particle size distribution determined by DLS; (d) Zeta potential of the AgNP colloidal system

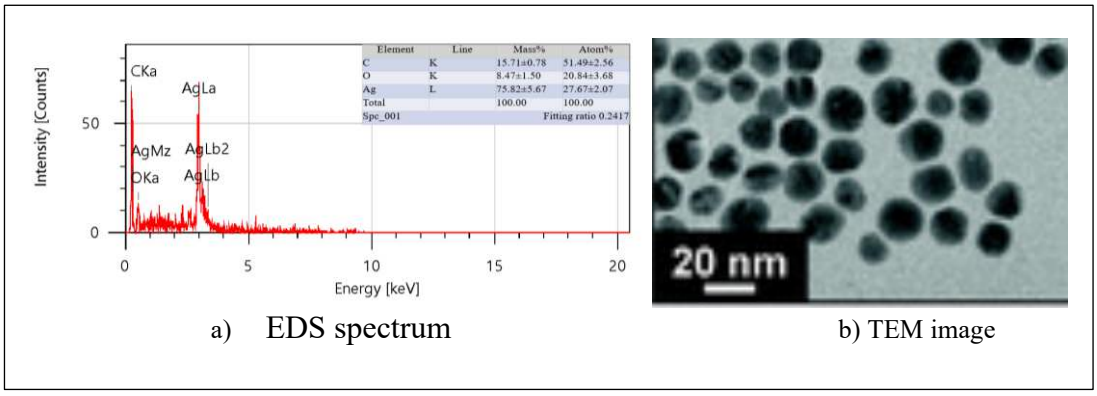


Fig. 7. (a): EDS spectrum of silver nanoparticles synthesized using *Adenosma caeruleum* extract; (b): TEM image of synthesized silver nanoparticles by *Adenosma caeruleum* extract.

Dynamic light scattering analysis showed that the synthesized AgNPs possessed a narrow particle size distribution with an average hydrodynamic diameter in the nanoscale range. Zeta potential measurements indicated a negative surface charge, reflecting good electrostatic repulsion between particles and excellent colloidal stability. The stability of the AgNPs can be attributed to the

adsorption of negatively charged phytochemicals on the nanoparticle surface, preventing aggregation and sedimentation.

3.3. Antibacterial and antifungal activities

The biosynthesized AgNPs exhibited pronounced antimicrobial activity toward both Gram-negative and Gram-positive bacteria, as well as the yeast *Candida albicans*, as illustrated in **Fig. 8 and Table 2**. Such broad-spectrum efficacy is generally attributed to multiple complementary mechanisms, including nanoparticle adhesion to microbial surfaces, disruption of membrane integrity, intracellular penetration, interaction with proteins and DNA, and induction of oxidative stress.

The agar well diffusion assay revealed a clear dose-dependent response. The progressive enlargement of inhibition zones with increasing sample volumes from 10 to 30 µL, as evidenced by **Fig. 8**, confirms that greater nanoparticle exposure leads to stronger microbial suppression. Importantly, visible halos exceeding the original well diameter (6 mm) were already observed at 10 µL, further supporting effective antimicrobial activity at low concentrations.

Gram-negative bacteria, particularly *Escherichia coli* (**Fig. 8a**) and *Salmonella typhimurium* (**Fig. 8b**), demonstrated higher susceptibility, as evidenced by the more pronounced expansion of inhibition zones at elevated volumes. This enhanced sensitivity is plausibly related to differences in cell wall organization; the thinner peptidoglycan layer may facilitate nanoparticle interaction and Ag^+ diffusion. In contrast, *Bacillus cereus* and *Staphylococcus aureus* (**Fig. 8c,d**) remained consistently inhibited, yet the magnitude of zone enlargement was less dramatic, suggesting that the thicker peptidoglycan barrier may partially limit nanoparticle penetration.

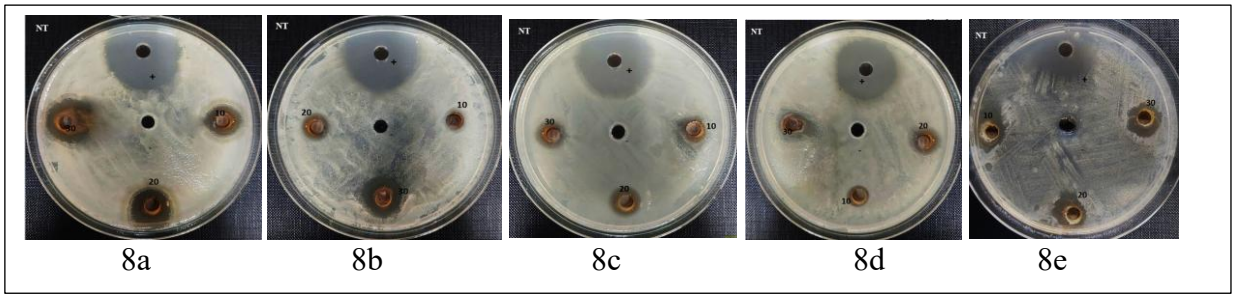


Fig. 8. a): Antimicrobial activity of silver nanoparticles against Escherichia coli, b): *Salmonella typhimurium,* c):*Bacillus cereus,* d): *Staphylococcus aureus, and* e): *Candida albicans.*

For *Candida albicans* (**Fig. 8e**), moderate inhibition was detected, and only a slight increase in halo size was recorded with increasing dosage, as illustrated in **Fig. 8e**. This observation indicates

that although antifungal activity is present, the AgNPs exhibit greater effectiveness toward bacterial cells. Membrane damage, enzyme inactivation, and disruption of cellular integrity are considered key contributors to the antifungal mechanism.

Table 2: Results of antibacterial testing of silver nanoparticles

No.	**Control** **Chloramphenicol (20µg)**	**Bacterial strain**	**Concentration(mg/mL)**	**Antibacterial diameter(mm)**
1	32.0 ± 0.5	*Escherichia coli*	10	11
			20	19
			30	21
2	25.0 ± 0.7	*Salmonella typhimurium*	10	8
			20	12
			30	22
3	28.0 ± 0.2	*Staphylococcus aureus*	10	11
			20	13
			30	14
4	28.0 ± 0.4	*Bacillus cereus*	10	10
			20	12
			30	14
5	22.2 ± 0.7	*Candida albicans*	10	11
			20	11.5
			30	12

The MIC determination further substantiated the diffusion results. The identical MIC value of 1.25 mg/mL obtained for all strains, as shown in **Fig. 9**, demonstrates stable and reproducible inhibitory capability across different microorganisms. Nevertheless, comparison with the positive control chloramphenicol (**Fig. 9**) indicates that the nanoparticle system remains less potent than the conventional antibiotic. Therefore, while not a direct substitute for standard drugs, these biosynthesized AgNPs hold promise for complementary applications and for the development of alternative or synergistic antimicrobial strategies.

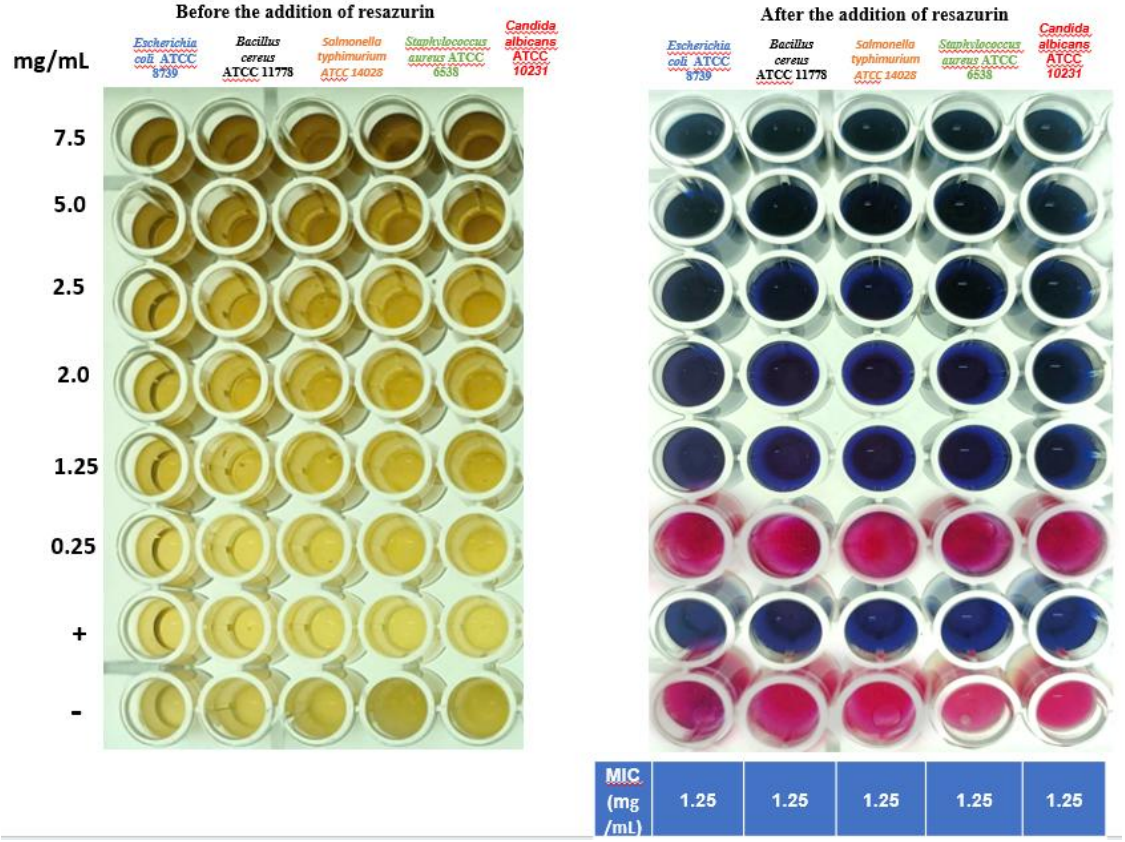


Fig. 9. Comparison of MIC values of the samples prior to and following resazurin addition

3.4. Antioxidant activity

The antioxidant potential of the biosynthesized AgNPs was assessed using the ABTS radical scavenging assay. The nanoparticles exhibited a clear concentration-dependent activity, confirming their ability to effectively quench free radicals. This behavior is commonly associated with the presence of phytochemical residues from the plant extract adsorbed on the nanoparticle surface, which may act synergistically with silver to enhance electron- or hydrogen-donating capacity. Such cooperation between the metallic core and bioactive capping agents represents a distinctive advantage of green-synthesized nanomaterials over those produced via purely chemical routes.

The Trolox standard displayed a gradual increase in radical scavenging efficiency with increasing concentration, ranging from 34.80% to 111.41% over 5–100 ppm, as illustrated in **Fig. 10 and Table 3** Linear regression analysis produced the equation $y = 0.7945x + 36.5223$ with a strong correlation coefficient ($R^2 \approx 0.974$), indicating excellent agreement between the experimental data

and the fitted model. Based on this relationship, the IC_{50} value of Trolox was calculated to be 16.96 µg/mL, reflecting its well-established high antioxidant potency. This value serves as a reference benchmark for evaluating the performance of the AgNPs.

For the nanoparticle sample, the IC_{50} determined from the ABTS assay was 49.8 µg/mL, as evidenced in **Fig. 11** and **Table 4**, demonstrating a fairly strong radical scavenging capability. Although the activity is lower than that of Trolox, the result remains notable considering that the reducing and stabilizing agents originate from natural plant metabolites. The findings suggest that the phytochemical corona surrounding the AgNPs plays a crucial role in modulating antioxidant behavior and may contribute to additional biological functionalities.

Table 3: Results of constructing the Trolox calibration curve

Trolox			
C (ppm)	**A_i**	**$SC_{ABTS^{\cdot+}}$**	**IC_{50} (µg/ml)**
5	0.463	34.8	16.96
25	0.29	59.15	
50	0.127	82.1	
75	0.016	97.75	
100	-0.081	111.41	

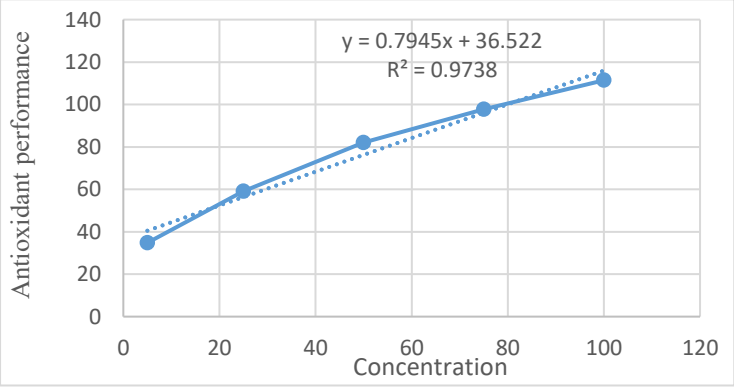


Fig. 10: Trolox calibration curve used to determine $ABTS^{+}$ reduction capability

Table 4: Results of antioxidant activity testing of silver nanoparticles

AgNPs			
C(ppm)	**A_i**	**$SC_{ABTS^{\cdot+}}$**	**IC_{50} (µg/ml)**

10	0.415	40.7	49.8
25	0.394	43.71	
50	0.34	51.43	
100	0.28	60	
200	0.15	78.57	

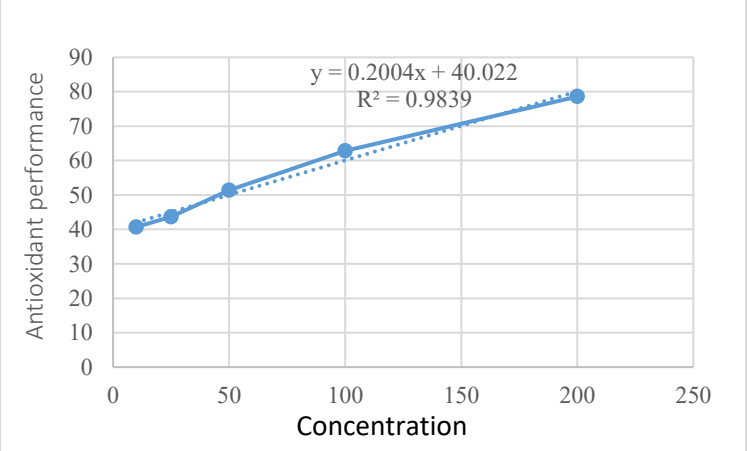


Fig. 11: $ABTS^{\cdot+}$ free radical scavenging ability of AgNPs

4. CONCLUSIONS

Silver nanoparticles were successfully synthesized via an environmentally friendly route using the plant extract as both reducing and stabilizing agents. Multiple techniques (UV–Vis, TEM, DLS, XRD, FTIR, and EDX) confirmed the formation of crystalline and well-dispersed particles with sizes mainly in the 20–50 nm range. The AgNPs displayed strong broad-spectrum antimicrobial activity against *E. coli, S. typhimurium, B. cereus, S. aureus,* and *C. albicans*, with inhibition zones up to 22 mm and a uniform MIC of 1.25 mg/mL, while Gram-negative strains were generally more sensitive. The nanoparticles also exhibited considerable antioxidant capacity with an ABTS IC_{50} of 49.8 µg/mL. These combined properties demonstrate the potential of the biosynthesized AgNPs as promising multifunctional agents for biomedical applications.

ACKNOWACKNOWLEDGMENT

We sincerely appreciate the support of the Faculty of Chemical Engineering, Industrial University of Ho Chi Minh City for their invaluable assistance in conducting this experiment.

ECLARATIONS

Ethical Approval

This study does not involve human participants or animals. Therefore, ethical approval was not required.

Consent to Participate

Not applicable.

Consent to Publish

All authors have reviewed the manuscript and approved the final version for publication.

Authors Contributions

Van Son Nguyen: Conceptualization, methodology, supervision, writing – original draft, writing review and editing.Thanh Cong Vo: Investigation, data curation, formal analysis. Thanh Khue Van: Experimental work, data analysis.The Ky Vo: Visualization, validation. All authors have read and approved the final manuscript.

Funding

This research received no external funding.

Competing Interests

The authors declare that they have no competing interests.

Availability of Data and Materials

The datasets generated and analyzed during the current study are available from the corresponding author on reasonable request.

REFERENCES

1. Ranjbar, R.; Alam, M.; Antimicrobial Resistance Collaborators. Global burden of bacterial antimicrobial resistance in 2019: a systematic analysis. *Evidence-Based Nursing*, 2023, 27, 16. https://doi.org/10.1136/ebnurs-2022-103540
2. Ventola, C. L. The antibiotic resistance crisis: Part 1: Causes and threats. *P&T*, 2015, 40, 277–283.
3. Davies, J.; Davies, D. Origins and evolution of antibiotic resistance. *Microbiology and Molecular Biology Reviews*, 2010, 74, 417–433. https://doi.org/10.1128/MMBR.00016-10
4. Roco, R.; Bainbridge, C. Societal implications of nanoscience and nanotechnology. *Nanoparticle Research*, 2005, 7, 1–13.
5. Meher, A.; Tandi, A.; Moharana, S.; Chakroborty, S.; Mohapatra, S. S.; Mondal, A.; Dey, S.; Chandra, P. Silver nanoparticle for biomedical applications: A review. *Hybrid Advances*, 2024, 6, 100184. https://doi.org/10.1016/j.hybadv.2024.100184

6. Morones, J. R.; Elechiguerra, J. L.; Camacho, A.; Holt, K.; Kouri, J. B.; Ramírez, J. T.; Yacaman, M. J. The bactericidal effect of silver nanoparticles. *Nanotechnology*, 2005, 16, 2346–2353. https://doi.org/10.1088/0957-4484/16/10/059

7. Prabhu, S.; Poulose, E. K. Silver nanoparticles: Mechanism of antimicrobial action, synthesis, medical applications, and toxicity effects. *International Nano Letters*, 2012, 2, 32. https://doi.org/10.1186/2228-5326-2-32

8. Rai, M.; Yadav, A.; Gade, A. Silver nanoparticles as a new generation of antimicrobials. *Biotechnology Advances*, 2009, 27, 76–83. **DOI:** https://doi.org/10.1016/j.biotechadv.2008.09.002

9. Li, Y.; Leung, X.; Yao, A.; Song, Z.; Newton, E. Antimicrobial effect of surgical masks coated with nanoparticles. *Journal of Hospital Infection*, 2006, 62, 58–63. **DOI:** https://doi.org/10.1016/j.jhin.2005.04.015

10. Ahmed, S.; Ahmad, M.; Swami, B. L.; Ikram, S. A review on plants extract mediated synthesis of silver nanoparticles for antimicrobial applications. *Journal of Advanced Research*, 2016, 7, 17–28. https://doi.org/10.1016/j.jare.2015.02.007

11. Sharma, V. K.; Yngard, R. A.; Lin, Y. Silver nanoparticles: Green synthesis and their antimicrobial activities. *Advances in Colloid and Interface Science*, 2009, 145, 83–96. **DOI:** https://doi.org/10.1016/j.cis.2008.09.002

12. Iravani, S. Green synthesis of metal nanoparticles using plants. *Green Chemistry*, 2011, 13, 2638–2650. https://doi.org/10.1039/C1GC15386B

13. Rafique, M.; Sadaf, I.; Rafique, M. S.; Tahir, M. B. A review on green synthesis of silver nanoparticles and their applications. *Artificial Cells, Nanomedicine, and Biotechnology*, 2017, 45, 1272–1291. **DOI:** https://doi.org/10.1080/21691401.2016.1241792

14. Singh, R.; Shedbalkar, U. U.; Wadhwani, S. A.; Chopade, B. A. Bacteriagenic silver nanoparticles: Synthesis, mechanism, and applications. *Applied Microbiology and Biotechnology*, 2016, 100, 2555–2566. **DOI:** https://doi.org/10.1007/s00253-015-7118-x

15. Anastas, P. T.; Warner, J. C. *Green Chemistry: Theory and Practice*. New York: Oxford University Press, 1998.

16. Singh, P.; Kim, Y. J.; Zhang, D.; Yang, D. C. Biological synthesis of nanoparticles from plants and microorganisms. *Trends in Biotechnology*, 2016, 34, 588–599. **DOI:** https://doi.org/10.1016/j.tibtech.2016.02.006

17. Mittal, S.; Chisti, A.; Banerjee, U. C. Synthesis of metallic nanoparticles using plant extracts. *Biotechnology Advances*, 2013, 31, 346–356. **DOI:** https://doi.org/10.1016/j.biotechadv.2013.01.003

18. Jannathul Firdhouse, M.; Lalitha, P. Biosynthesis of silver nanoparticles using plant extracts and their antimicrobial activities. *Journal of Nanostructure in Chemistry*, 2015, 5, 341–351. **DOI:** https://doi.org/10.1007/s40097-015-0171-3

19. Iravani, S.; Varma, R. S. Green synthesis, biomedical and biotechnological applications of silver nanoparticles. *Environmental Chemistry Letters*, 2020, 18, 703–727. **DOI:** https://doi.org/10.1007/s10311-020-00952-3

20. Chi, V. V. *Từ điển cây thuốc Việt Nam*. Hà Nội: Nhà xuất bản Y học, 2012.

21. Hien, N. T.; Huong, N. T. Phytochemical constituents of *Adenosma caeruleum* R.Br. *Vietnam Journal of Chemistry*, 2014, 52, 89–94.

22. Nguyen, T. T.; Tran, P. H. Coumarins and flavonoids from *Adenosma caeruleum* and their antioxidant activity. *Natural Product Communications*, 2016, 11, 103–106. DOI: https://doi.org/10.1177/1934578X1601100129

23. Khandelwal, S.; Sharma, N.; Tiwari, A. Plant-mediated silver nanoparticles and their antioxidant potential. *Materials Science and Engineering C*, 2018, 93, 999–1006. **DOI:** https://doi.org/10.1016/j.msec.2018.08.060

March 27, 2026